HENSARD JOURNAL OF ENVIRONMENT

HJ

Article

Geospatial Analysis of LULC change during 2001-2022, Nigeria.

Zubairul Islam [1], Kebiru Omoru[1,2] Jaspal Singh[3] Anamika Agarwal[3], Ravi Kumar Gangwar[4]*, Gaurav Bhushan[3], Sameer Chandra[4]

Academic Editor: Prof. Rashid Faridi

Received: 10.08.2025
Revised: 10.11.2025
Accepted: 28.11.2025
Published: 05.12.2025

Citation: Islam, Z., Omoru, K., Singh, J., Agarwal, A., & Gangwar, R. K. (2025). *Geospatial analysis of LULC change during 2001–2022, Nigeria*. **Hensard Journal of Environment**, 1(1).

[1] Faculty of Environmental Sciences, Hensard University, Toru-Orua, Sagbama Local Government Area, Bayelsa, Nigeria 561001, Nigeria
[2] The National Centre for Remote sensing Jos (NCRS), Nigeria. kabirchief@yahoo.com
[3] Department of Environmental Science, Bareilly College, Bareilly, U.P. India Jaspalsingh_lko@yahoo.co.in
[4] Biotechnology Section, ICAR-Indian Veterinary Research Institute (Deemed University), Bareilly, U.P. India ravi25388@gmail.com
[4] Department of Botany, School of Sciences, IFTM University, Moradabad, U. P., India.

* Correspondence: ravi25388@gmail.com

Abstract

Reliable, spatially explicit evidence on land-cover change is essential for climate adaptation, agricultural planning, and monitoring of SDG targets in West Africa. We map and quantify national-scale land-cover dynamics in Nigeria between 2000/2001 and 2022 using the ESA C3S/CCI Land Cover Level-4 product (300 m). Annual categorical layers were assembled and harmonized in Google Earth Engine, clipped to the GAUL Level-0 boundary, and stacked as LC_<YYYY>. To preserve class integrity, we applied nearest-neighbor resampling for grid alignment, masked no-data (0), and restricted accounting to "present classes only." We computed per-class areas, net changes, and a pixel-wise transition matrix, and summarized transitions into policy-oriented groups (e.g., forest/savanna → cropland; cropland → urban; stable). Results show broad national stability with targeted reconfiguration. Rainfed cropland and woody savanna/deciduous cover dominate both epochs; nonetheless, rainfed cropland expanded modestly at the national scale, urban land approximately tripled in share (from ~0.3% to ~1.1%), and woody vegetation reorganized toward more open/deciduous physiognomies. Shrub and grass classes contracted, while permanent water remained largely stable at 300 m. Dominant flows include shrubland/grassland → cropland and cropland/mosaics → urban near major corridors, alongside internal shifts among woody classes across the Sudanian–Guinean belt. Cross-sensor validation with MODIS MCD12Q1 (IGBP) indicates only moderate agreement after legend grouping, reflecting differences in spatial resolution, seasonality, and ontologies; accuracy improves when restricting to homogeneous cores and coarser support, framing discrepancies as uncertainty bounds rather than simple error. The workflow provides a reproducible national evidence base for Nigeria, suitable for routine monitoring and state-level planning. Findings highlight the need to balance cropland expansion and rapid urban growth with ecosystem connectivity, flood mitigation, and restoration in savanna regions. Future work should integrate multi-sensor fusion, probabilistic agreement metrics, and driver analyses to strengthen attribution and decision relevance.

Keywords: land-cover change; Nigeria; ESA C3S/CCI; Google Earth Engine; transition matrix; cropland expansion; urbanization; savanna dynamics; cross-sensor validation.

1. Introduction

Land-cover change is a primary driver and indicator of environmental transformation, shaping water availability, food security, biodiversity, and climate risk (Li et al., 2018; Li et al., 2022). In

West Africa, and Nigeria in particular, rapid population growth, agricultural expansion, and accelerating urbanization have intensified pressures on land systems over the last two decades (Herrmann et al., 2020; UNCCD, 2023). These pressures are spatially heterogeneous—concentrated along transport corridors and peri-urban belts, yet also diffuse across cropland–savanna mosaics and floodplains (Koko et al., 2021; Yin et al., 2021). Reliable, spatially explicit evidence of how land cover has changed at national scale is therefore essential for planning climate adaptation, guiding agricultural policy, and monitoring progress toward land-related SDGs (UN DESA, 2021; Akinyemi et al., 2022).

This study maps and quantifies national-scale land-cover dynamics in Nigeria between 2000/2001 and 2022 using the ESA C3S/CCI Land Cover Level-4 (300 m) product assembled and harmonized in Google Earth Engine (C3S, 2025; ESA CCI, 2017; Gorelick et al., 2017). We generate an annual, temporally ordered LC_<YYYY> stack for Nigeria, estimate per-class areas, compute net changes, and derive a pixel-wise transition matrix. To aid interpretation, we also distill transitions into a simplified set of cross-group categories (e.g., forest/savanna → cropland; cropland → urban; stable), and produce cartographic outputs with administrative overlays suitable for policy-facing communication.

Despite widespread use of Earth-observation products in Africa, robust, nationally consistent, and methodologically transparent evidence on recent Nigerian land-cover trajectories remains scarce. Official statistics alone cannot capture fine-scale spatial patterns (e.g., peri-urban expansion, cropland encroachment into woody savannas, or localized wetland changes); a consistent remote-sensing baseline is necessary to (i) quantify the magnitude and direction of change, (ii) identify where transitions cluster geographically, and (iii) benchmark future monitoring under increasing climatic variability (Herrmann et al., 2020; UNCCD, 2023; Yin et al., 2021)..

To the best of our knowledge, no recent study provides a Nigeria-wide, 300 m-resolution transition accounting from 2000/2001 to 2022 using the C3S/CCI L4 legend with explicit handling of absent classes and grid harmonization. We address this gap by asking: (1) What is the magnitude and composition of land-cover change across Nigeria between 2000/2001 and 2022? (2) Which transitions dominate (e.g., woody vegetation → cropland; cropland → urban), and where are they spatially concentrated? (3) How much of the landscape remains stable? (4) How do simplified cross-group transitions clarify policy-relevant narratives relative to the full legend?

Methodologically, we contribute a reproducible GEE-based workflow that (i) standardizes yearly naming (LC_<YYYY>), (ii) preserves categorical integrity via nearest-neighbor resampling and common-extent alignment, (iii) restricts metrics to "present classes only" to avoid denominator inflation, and (iv) encodes pixel-level transitions for diagnostic mapping. Substantively, we deliver a national evidence base on where and how Nigeria's land surface has changed—quantifying cropland expansion and urban growth, documenting restructuring within woody and shrub/grass classes, and delineating stable areas. The outputs support land-use planning, climate adaptation targeting, and future cross-sensor validation and trend attribution.

2. Materials and Methods

2.1 Study area

Nigeria (≈923,768 km²; 36 states and the Federal Capital Territory) spans West Africa from the Gulf of Guinea to the southern Sahel, approximately 4–14° N and 3–15° E. The national territory encompasses a strong meridional hydro-climatic gradient: humid coastal and sub-equatorial conditions in the south give way to sub-humid Guinean and Sudanian savannas in the center and semi-arid Sahelian zones in the far north. Mean annual rainfall increases from roughly <700 mm in the north to >2,000 mm in parts of the south and Niger Delta, with growing seasons ranging from ~3–4 months (north) to ~8–9 months (south). Temperatures are uniformly warm (typically 26–28 °C annually) but seasonality in moisture and the West African monsoon strongly structure vegetation phenology, fire regimes, and land-use calendars.

Topographically, Nigeria is dominated by lowlands (<500 m a.s.l.) interrupted by uplands such as the Jos Plateau (~1,200–1,400 m) and the Adamawa Highlands. The fluvial network is anchored by the Niger and Benue rivers, which meet at Lokoja and drain a mosaic of floodplains, freshwater swamps, and coastal mangroves. Ecologically, the country spans lowland rainforests and mangrove/wetland complexes in the south, a broad savanna belt (wooded and open) across the center, and shrub/grass systems grading to Sahel in the north. This environmental diversity underpins a corresponding diversity of land systems—from perennial tree crops and mixed rainfed smallholder agriculture to extensive rangelands—making Nigeria an informative natural laboratory for detecting and attributing land-cover change.

For this study, the area of interest (AOI) is the sovereign boundary of Nigeria as defined by GAUL 2015 Level-0. All annual land-cover layers were clipped to this boundary to avoid edge artifacts, and administrative level-1 units (states) are used for cartographic context and optional stratification of summary statistics. This combination of clear administrative limits and strong biophysical gradients supports both national accounting of change and interpretation of spatial patterns in relation to climate, terrain, and settlement corridors.

.

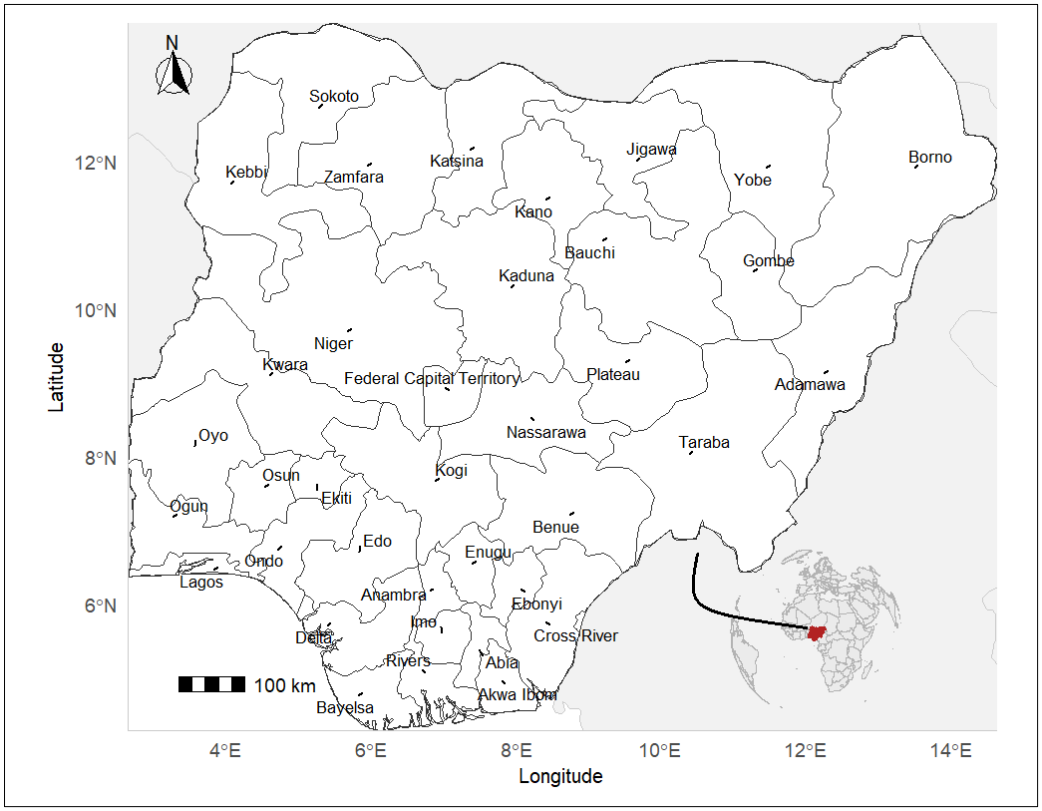

Figure 1. Maps showing the study area.

2.2 Land-cover data and preprocessing

We used the **ESA C3S/CCI Land Cover Level-4 (LCCS)** collection (*projects/sat-io/open-datasets/ESA/C3S-LC-L4-LCCS*) at 300 m spatial resolution (ESA CCI, 2017; Li et al., 2018). In **Google Earth Engine (GEE)**, we restricted the analysis to **Nigeria** using the **GAUL 2015 Level-0 national boundary** (*FAO/GAUL/2015/level0*, filtered to `ADM0_NAME = "Nigeria"*) and centered the map on the area of interest (FAO, 2015). From each image in the collection, we selected the categorical land-cover band *b1* (LCCS class codes). Because the collection's *system:index* encodes the acquisition year, we parsed the four-digit year from that string and attached it to each image as a property (yy) (Gorelick et al., 2017). We then (i) enumerated all available years, (ii) for

each year selected the first image with matching yy, (iii) retained *b1*, and (iv) renamed it to *LC_<YYYY>* (e.g., *LC_2018*). Each yearly image was clipped to the Nigeria boundary to avoid edge artifacts.

All annual layers were concatenated into a single, temporally ordered multi-band stack using toBands(), and the band names were explicitly set to the sorted *LC_<YYYY>* sequence to ensure stable, unambiguous indexing across years (Broxton et al., 2014). The land-cover values follow the **C3S/CCI LCCS code list** (nominal range 10–220); pixels with value 0 (no data) were treated as missing in downstream analysis. No radiometric transformations were required for this categorical product; where resampling was necessary (e.g., for visualization or alignment with other rasters), we used nearest-neighbor interpolation to preserve class integrity (Defourny et al., 2019). The native map projection supplied by the collection was maintained throughout; all vector overlays (administrative boundaries) were reprojected on the fly to match the raster CRS (C3S, 2025). A quick-look layer of the most recent band (*LC_<latest year>*) was added for quality control, but all metrics and figures in the manuscript were derived from the stacked categorical bands..

2.3 Change analysis from multi-year C3S/CCI stack ("present classes only")

We quantified land-cover change between 2000 and 2022 from the ESA C3S/CCI Level-4 stack by (i) selecting the target-year bands (*LC_2000*, *LC_2022*), (ii) harmonizing their grids, and (iii) computing areas and transitions only for classes that actually occur in either year (absent classes are dropped to avoid zero rows/columns and inflated denominators) (Li et al., 2022; Herrmann et al., 2020).

Pre-processing. he raster stack was read with *terra* (Hijmans, 2023). Pixels coded 0 (no data) were set to NA. The 2022 band was reprojected to the 2000 grid using nearest-neighbor to preserve categorical values. The common extent was intersected and both rasters were cropped accordingly. Per-cell area (km²) was computed from the 2000 grid.

Per-class areas. For each year, area totals by LCCS class were obtained with zonal(area_km2, class_raster, "sum"). Only codes present in 2000 or 2022 were retained ("present classes only"). Class names followed the official C3S legend (ESA CCI, 2017).

Net change. Areas for 2000 and 2022 were joined by class to derive absolute and relative net change (Bontemps et al., 2013):

$$\Delta \boldsymbol{A}_{\boldsymbol{km^2}} = \boldsymbol{A}_{\boldsymbol{2022}} - \boldsymbol{A}_{\boldsymbol{2000}}, \qquad \Delta\% \frac{\Delta \boldsymbol{A}}{\boldsymbol{max}(\boldsymbol{A}_{\boldsymbol{2000}}, \in)}$$

Transition matrix. Pixel-wise transitions were encoded as

$$\boldsymbol{pair} = \mathbf{100} \times \boldsymbol{LC}_{\mathbf{2000}+}\boldsymbol{LC}_{\mathbf{2022}}$$

Summing area_km2 by pair yielded transition areas (km²), which were reshaped into a square matrix **restricted to the present codes**. Totals of unchanged area were taken from the matrix diagonal; changed area equals total minus diagonal (Hansen et al., 2013).

3. Results

3.1. Land-cover change, 2001–2022 (C3S/CCI, Nigeria)

C3S/CCI maps show that Nigeria's land surface in both 2001 and 2022 was dominated by rainfed cropland and open deciduous broad-leaved tree cover (Fig. 2; Table 2).

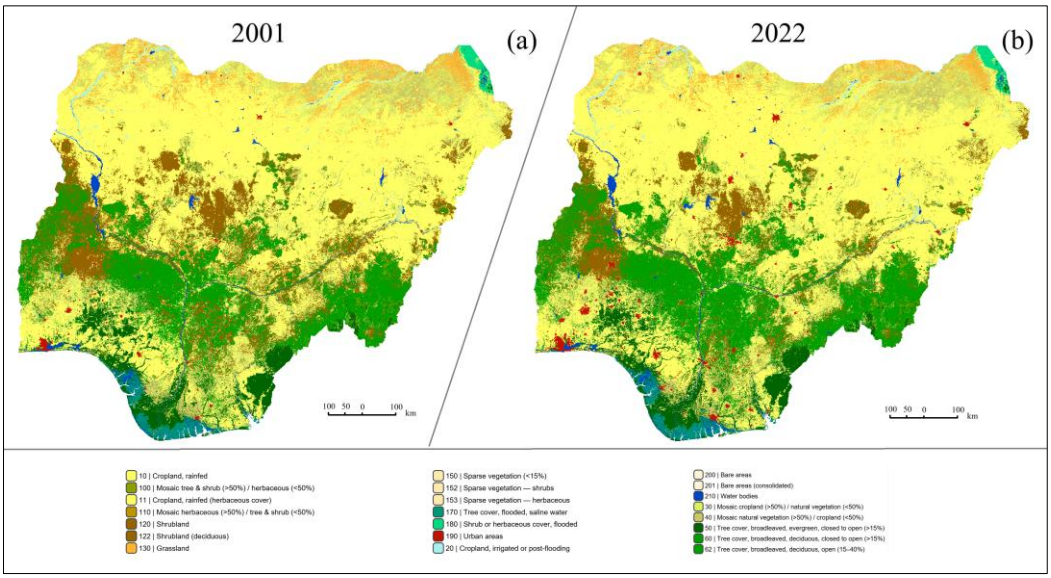

Figure 2. ESA C3S/CCI Land-Cover (LCCS) maps of Nigeria at 300 m resolution for (a) 2001 and (b) 2022. Classes follow the C3S/CCI L4 legend (see legend below each map); no-data (0) was masked. Data: ESA C3S/CCI LULC (Level-4).

Code	Class (C3S/CCI LCCS)	Area 2001 (km²)	Share 2001 (%)	Area 2022 (km²)	Share 2022 (%)
10	Cropland, rainfed	350154.81	38.471	357635.33	39.293
11	Cropland, rainfed (herbaceous cover)	59622.86	6.551	65842.29	7.234
20	Cropland, irrigated or post-flooding	6869.14	0.755	6956.12	0.764
30	Mosaic cropland (>50%) / natural vegetation (<50%)	79763.82	8.764	81331.06	8.936
40	Mosaic natural vegetation (>50%) / cropland (<50%)	62986.82	6.920	59989.45	6.591
50	Tree cover, broadleaved, evergreen, closed to open (>15%)	42504.69	4.670	43162.15	4.742
60	Tree cover, broadleaved, deciduous, closed to open (>15%)	2648.29	0.291	18067.77	1.985
62	Tree cover, broadleaved, deciduous, open (15–40%)	127398.54	13.997	134299.96	14.755
100	Mosaic tree & shrub (>50%) / herbaceous (<50%)	3097.92	0.340	3658.39	0.402
110	Mosaic herbaceous (>50%) / tree & shrub (<50%)	165.93	0.018	176.47	0.019
120	Shrubland	106380.37	11.688	70046.84	7.696
122	Shrubland (deciduous)	11921.09	1.310	9465.30	1.040
130	Grassland	30956.73	3.401	25910.29	2.847
150	Sparse vegetation (<15%)	111.38	0.012	489.45	0.054
152	Sparse vegetation — shrubs	0.35	0.000	0.35	0.000
153	Sparse vegetation — herbaceous	355.58	0.039	302.98	0.033
170	Tree cover, flooded, saline water	8749.69	0.961	8702.97	0.956
180	Shrub or herbaceous cover, flooded	3763.44	0.413	3751.02	0.412
190	Urban areas	2828.54	0.311	9918.49	1.090
200	Bare areas	114.17	0.013	170.43	0.019
201	Bare areas (consolidated)	26.23	0.003	24.37	0.003
210	Water bodies	9761.84	1.073	10280.74	1.130
	Total	910182.20	100.00	910182.20	100.00

Between 2001 and 2022 the total mapped area remained constant (≈ 910,182 km²), but class composition shifted in several important ways:

- Cropland expanded modestly overall. Rainfed cropland increased from 350,155 km² (38.47%) to 357,635 km² (39.29%) (+7,481 km²; +0.82 pp). The herbaceous rainfed subclass rose by +6,219 km² (+0.68 pp). Irrigated/post-flood cropland remained small and stable (+87 km²; +0.01 pp). Mosaic cropland > 50% also grew (+1,567 km²; +0.17 pp), while the reciprocal mosaic (natural > 50%) declined (−2,997 km²; −0.33 pp).
- Woody vegetation shifted toward deciduous/open structure. "Tree—broadleaf, deciduous, closed-to-open" rose sharply from 2,648 km² (0.29%) to 18,068 km² (1.99%) (+15,419 km²; +1.70 pp), and the "deciduous, open (15–40%)" class increased by +6,901 km² (+0.76 pp). Evergreen broadleaf cover changed little (+657 km²; +0.07 pp).
- Shrub and grass classes contracted. Shrubland decreased by −36,334 km² (−3.99 pp); deciduous shrubland by −2,456 km² (−0.27 pp); and grassland by −5,046 km² (−0.55 pp). Sparse vegetation remained minor (net +378 km²; +0.04 pp across subclasses).
- Urban area nearly tripled in share. Urban pixels increased from 2,829 km² (0.31%) to 9,918 km² (1.09%) (+7,090 km²; +0.78 pp), consistent with rapid settlement growth observed along major corridors.
- Aquatic and flooded classes were stable. Water bodies grew slightly (+519 km²; +0.06 pp), while flooded vegetation (saline and shrub/herb) changed by < 50 km² in total (≤ ±0.01 pp).
- Bare land remained rare. Bare areas increased marginally (+56 km²; +0.01 pp), and consolidated bare decreased by −1.9 km².

3.2. Class persistence and dominant flows (2001–2022)

The transition matrix indicates that the majority of pixels remained in their original class between 2001 and 2022, with the largest stable blocks in rainfed cropland (10→10, 341.5×10³ km²), open deciduous broad-leaved trees (62→62, 126.1×10³ km²), cropland-dominated mosaics (30→30, 74.4×10³ km²), shrubland (120→120, 67.0×10³ km²), grassland (130→130, 25.3×10³ km²) and water (210→210, 9.51×10³ km²). These diagonal terms corroborate the visual persistence noted in the maps.

Beyond persistence, several directional transitions structure the landscape change:

- Cropland gains. Gross inflow to rainfed cropland was dominated by shrubland→cropland (120→10, 12.50×10³ km²) and grassland→cropland (130→10, 2.42×10³ km²), with smaller inputs from mosaic/natural classes. These fluxes explain the net areal increase in cropland reported in Table 2.
- Cropland losses and urbanization. The largest outflow from cropland was cropland→urban (10→190, 3.29×10³ km²), followed by conversion to woody and shrub classes (10→60, 2.38×10³ km²; 10→50, 1.02×10³ km²; 10→120, 1.33×10³ km²). Urban expansion also drew from mosaics (30→190, 0.84×10³ km²) and natural mosaics (40→190, 1.02×10³ km²).
- Woody-vegetation restructuring. Shrubland exported substantial area to tree and cropland classes—to deciduous broad-leaved (closed-to-open) (120→60, 6.91×10³ km²), to deciduous open (120→62, 7.59×10³ km²), and to cropland (120→10, 12.50×10³ km²)—indicating a reorganization toward cropland and more open tree physiognomies in the northern and central belts.
- Aquatic and flooded classes. Water and flooded classes were largely stationary (e.g., 210→210, 9.51×10³ km²; 170→170, 8.30×10³ km²), with modest exchanges (170→210, 0.162×10³ km²; 62→210, 0.074×10³ km²), consistent with limited long-term surface-water reconfiguration at the product's spatial resolution.

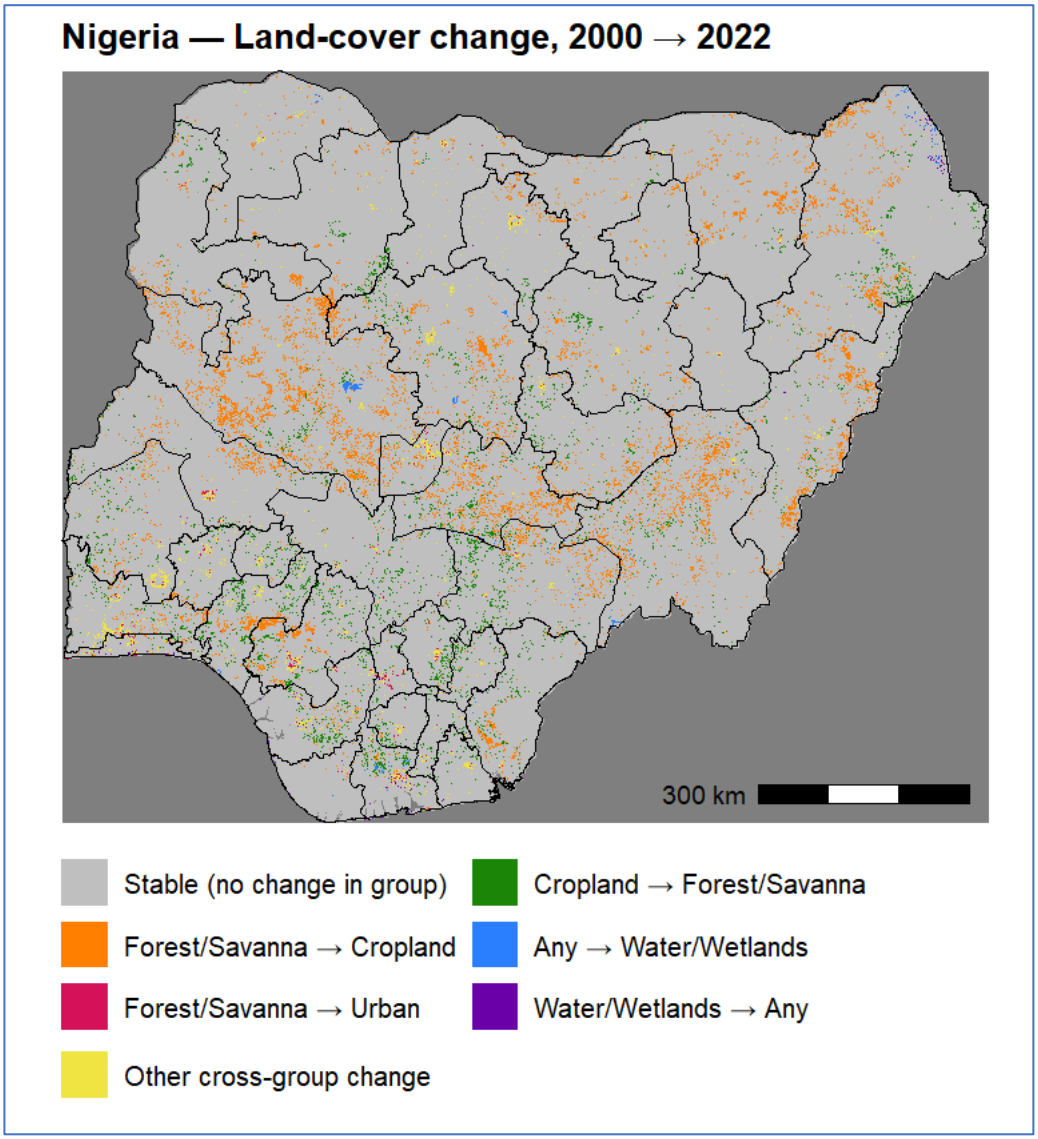

4. Discussion

Our national-scale assessment reveals a landscape that is largely persistent yet undergoing targeted, policy-relevant reconfiguration. Diagonal dominance in the transition matrix confirms widespread stability—especially in rainfed cropland, open deciduous broad-leaved cover, cropland-dominated mosaics, shrubland, grassland, and permanent water—consistent with long-standing agro-savanna land systems (Brandt et al., 2018; Leroux et al., 2021). Against this background, three directional flows structure Nigeria's recent land-cover dynamics (2000/2001–2022): (i) expansion of cropland at the expense of woody savanna and shrubland, (ii) conversion from cropland and mosaics to urban land, and (iii) internal restructuring within woody vegetation toward more open deciduous physiognomies. The cropland gains we report are modest in national share but spatially consequential, aligning with intensification around existing agricultural frontiers and along transport corridors (Funk et al., 2019; Samaké et al., 2023). Urban growth remains a small fraction of national area, yet its relative increase is large and concentrated near state capitals and peri-urban belts, with implications for heat exposure, flood risk, and prime-land loss (Oluseyi et al., 2020; Simwanda & Ranagalage, 2021).

The contraction of shrub and grass classes, together with gains in open/deciduous tree cover, suggests a complex interplay of cultivation pressure, wood extraction, and climatic variability that reorganizes savanna structure rather than producing wholesale forest loss (Andela et al., 2017; Nwosu et al., 2023). Such restructuring is most evident across the Sudanian–Guinean belt, where

seasonal moisture constraints and fire regimes interact with human use (Jiang et al., 2020). Aquatic and flooded classes are comparatively stable at 300 m, indicating that long-term reconfiguration of major water bodies has been limited relative to surrounding land-system changes; localized floodplain dynamics may nevertheless be under-represented at this resolution (Papa et al., 2010).

Methodologically, three choices were critical. First, restricting accounting to "present classes only" avoided denominator inflation and zero-rows/columns in the transition matrix, yielding more interpretable change magnitudes. Second, categorical integrity was preserved via nearest-neighbor resampling and common-extent alignment—essential for pixel-wise transitions but not eliminating mixed-pixel effects in ecotones. Third, the simplified change typology (e.g., forest/savanna → cropland; cropland → urban; stable) distilled a high-dimensional legend into policy-relevant narratives without suppressing underlying legend fidelity (Estel et al., 2020).

Cross-sensor validation with MODIS MCD12Q1 underscores the challenges of legend harmonization and scale. Even after grouping to comparable classes, overall agreement was modest—improving when filtered to homogeneous cores and aggregated to coarser support, yet remaining sensitive to resolution (300 m vs. 500–1,000 m), seasonality, and differing training ontologies (C3S LCCS vs. MODIS IGBP) (Sulla-Menashe & Friedl, 2018). These discrepancies should be interpreted as uncertainty bounds rather than simple error, especially in mosaicked landscapes and transition zones. Future work should incorporate probabilistic agreement metrics, temporal compositing windows, and region-specific correspondence tables to reduce semantic mismatch (Padarian et al., 2022).

Uncertainties persist. Mixed pixels and sub-class heterogeneity can bias transitions near class boundaries; interannual variability in phenology may toggle pixels across physiognomic thresholds (e.g., open vs. closed deciduous); and small but systematic geolocation differences can create spurious edge changes. While our workflow masks no-data, retains the native projection, and applies conservative resampling, remaining biases likely attenuate fine-scale signals and undercount narrow features (riparian strips, small wetlands). Incorporating multi-sensor fusion (e.g., Sentinel-2, Landsat ARD) and object-based approaches could sharpen edges and reduce speckle without sacrificing temporal coverage (Belgiu & Drăguţ, 2016; Midekisa et al., 2020).

The policy implications are direct. Continued cropland expansion into woody savannas highlights the need to balance production with landscape connectivity and soil conservation, particularly in erosion-prone northern states (Ibrahim et al., 2021). Rapid urban growth—though small in area—carries outsized impacts on heat, runoff, and infrastructure siting; integrating these maps into state-level land-use plans can help target green-space preservation and flood mitigation (Adeniyi et al., 2022). The documented stability of major water bodies at national scale provides a baseline for drought and dam-operation studies, while the observed restructuring within woody classes motivates targeted restoration and fire-management pilots in the savanna belt (Cochrane & Ryan, 2009).

5. Conclusions

This study delivers a high-resolution, building-level picture of geographic access to health We present a reproducible, national-scale assessment of Nigeria's land-cover change (2000/2001–2022) using ESA C3S/CCI (300 m), with harmonized annual stacks, nearest-neighbor resampling, and "present-classes-only" accounting for defensible area and transition estimates. The landscape is largely stable, but three directional shifts stand out: modest cropland expansion, rapid (though spatially concentrated) urban growth, and restructuring of woody savannas toward more open/deciduous classes; shrub/grass categories contract accordingly. Cross-sensor checks with MODIS highlight moderate agreement shaped by differences in resolution and legends, emphasizing uncertainty bounds rather than simple error. Policy priorities include managing cropland frontiers, planning for peri-urban growth (heat, runoff, loss of prime land), and targeted restoration/fire management in savanna belts. Future work should extend full-archive trajectories, integrate higher-resolution sensors, and adopt probabilistic validation to sharpen attribution and decision relevance.

Supplementary Materials: Available at https://github.com/zubairgis/nigeria-hensard

Author Contributions:

Z.I.: Conceptualization, Methodology, Supervision, Writing—original draft preparation, Writing—review and editing.
K.O.: Data curation, Formal analysis, Visualization, Writing—review and editing.
J.S.: Validation, Methodology, Writing—review and editing.
A.A.: Investigation, Resources, Writing—review and editing.
R.K.G.: Software, Data processing, Visualization, Writing—review and editing.

Funding: This research received no external funding.

Data Availability Statement: The satellite data used in this study are open to access as follows:

Administrative: https://developers.google.com/earth-engine/datasets/catalog/ FAO/GAUL/2015/level1
DEM:https://developers.google.com/earth-engine/datasets/catalog/ SGS/SRTMGL1_003
Roads & Water Routes: https://www.openstreetmap.org/#map=6/9.12/8.67
Landcover classes: https://land.copernicus.eu/en/global
Google Building Footprints: https://sites.research.google/gr/open-buildings/

Acknowledgments:

Conflicts of Interest: The authors declare no conflicts of interest.

Abbreviations

The following abbreviations are used in this manuscript:

Abbreviation	Full Term / Description
AOI	Area of Interest
ARD	Analysis Ready Data
C3S	Copernicus Climate Change Service
CCI	Climate Change Initiative (ESA)
CRS	Coordinate Reference System
ESA	European Space Agency
FAO	Food and Agriculture Organization of the United Nations
GAUL	Global Administrative Unit Layers
GEE	Google Earth Engine
IGBP	International Geosphere–Biosphere Programme (land-cover classification system)
LCCS	Land Cover Classification System
LC_	Annual Land-Cover Band (e.g., LC_2000, LC_2022)
LULC	Land Use and Land Cover
MODIS	Moderate Resolution Imaging Spectroradiometer
NDVI	Normalized Difference Vegetation Index
NOAA	National Oceanic and Atmospheric Administration
RGB	Red–Green–Blue (composite imagery)
SDG	Sustainable Development Goal
UNCCD	United Nations Convention to Combat Desertification
UN DESA	United Nations Department of Economic and Social Affairs
WGS84	World Geodetic System 1984 (spatial reference datum)

References

Adeniyi, O. S., Akinluyi, F. O., & Adeola, A. M. (2022). Urban expansion and surface temperature variability in major Nigerian cities using remote sensing and spatial metrics. Sustainable Cities and Society, 82, 103870. https://doi.org/10.1016/j.scs.2022.103870

Akinyemi, F. O., Mavengahama, S., & Sibanda, M. (2022). Agricultural landscape change impact on the quality of land: Evidence from Africa. Land Use Policy, 114, 105993. https://doi.org/10.1016/j.landusepol.2021.105993

Andela, N., Morton, D. C., Giglio, L., Chen, Y., van der Werf, G. R., Kasibhatla, P. S., ... & Randerson, J. T. (2017). A human-driven decline in global burned area. *Science, 356*(6345), 1356–1362. https://doi.org/10.1126/science.aam9247

Belgiu, M., & Drăguţ, L. (2016). Random forest in remote sensing: A review of applications and future directions. *ISPRS Journal of Photogrammetry and Remote Sensing, 114*, 24–31. https://doi.org/10.1016/j.isprsjprs.2016.01.011

Bontemps, S., Defourny, P., Van Bogaert, E., Arino, O., Kalogirou, V., & Perez, J. R. (2013). GLOBCOVER 2009—Products description and validation report. European Space Agency. https://due.esrin.esa.int/page_globcover.php

Brandt, M., Hiernaux, P., Tagesson, T., Verger, A., Rasmussen, K., Diouf, A. A., ... & Fensholt, R. (2018). Changes in rainfall distribution promote woody foliage production in the Sahel. *Environmental Research Letters, 13*(4), 044011. https://doi.org/10.1088/1748-9326/aabf53

Broxton, P. D., Zeng, X., Scheftic, W., & Troch, P. A. (2014). A MODIS-based global 1-km maximum green vegetation fraction dataset. Journal of Applied Meteorology and Climatology, 53(8), 1996–2004. https://doi.org/10.1175/JAMC-D-13-0356.1

Cochrane, M. A., & Ryan, K. C. (2009). Fire and fire ecology: Concepts and principles. In C. A. M. Prasad & A. R. Wiegand (Eds.), *Tropical Fire Ecology* (pp. 25–62). Springer. https://doi.org/10.1007/978-3-540-77381-8_2

Copernicus Climate Change Service (C3S). (2025). Land cover classification gridded maps from 1992 to present (quality & documentation page). https://cds.climate.copernicus.eu/datasets/satellite-land-cover

Copernicus Climate Change Service (C3S). (2025). Land cover classification gridded maps from 1992 to present (Version 3). Copernicus Climate Data Store. https://cds.climate.copernicus.eu/datasets/satellite-land-cover

Defourny, P., Lamarche, C., Bontemps, S., & Van Bogaert, E. (2019). ESA Climate Change Initiative Land Cover (CCI LC): Phase 3 final report. European Space Agency. https://climate.esa.int/en/projects/land-cover

ESA Climate Change Initiative (ESA CCI). (2017). Land Cover CCI—Product User Guide (Version 2.0). https://maps.elie.ucl.ac.be/CCI/viewer/download/ESACCI-LC-Ph2-PUGv2_2.0.pdf

Estel, S., Kuemmerle, T., Levers, C., Baumann, M., & Hostert, P. (2020). Mapping cropland-use intensity across Europe using MODIS NDVI time series. *Remote Sensing, 12*(3), 339. https://doi.org/10.3390/rs12030339

European Space Agency Climate Change Initiative (ESA CCI). (2017). Land Cover CCI: Product User Guide (Version 2.0). https://maps.elie.ucl.ac.be/CCI/viewer/download/ESACCI-LC-Ph2-PUGv2_2.0.pdf

Food and Agriculture Organization (FAO). (2015). Global Administrative Unit Layers (GAUL): Technical Aspects of the GAUL Dataset. FAO. https://data.apps.fao.org/map/catalog/srv/en/main.home

Funk, C., Peterson, P., Landsfeld, M., Pedreros, D., Verdin, J., Rowland, J., ... & Michaelsen, J. (2019). The climate hazards infrared precipitation with stations (CHIRPS) dataset. *Scientific Data, 6*, 210. https://doi.org/10.1038/s41597-019-0342-8

Gorelick, N., Hancher, M., Dixon, M., Ilyushchenko, S., Thau, D., & Moore, R. (2017). Google Earth Engine: Planetary-scale geospatial analysis for everyone. Remote Sensing of Environment, 202, 18–27. https://doi.org/10.1016/j.rse.2017.06.031

Gorelick, N., Hancher, M., Dixon, M., Ilyushchenko, S., Thau, D., & Moore, R. (2017). Google Earth Engine: Planetary-scale geospatial analysis for everyone. Remote Sensing of Environment, 202, 18–27. https://doi.org/10.1016/j.rse.2017.06.031

Hansen, M. C., Potapov, P. V., Moore, R., Hancher, M., Turubanova, S. A., Tyukavina, A., ... & Townshend, J. R. G. (2013). High-resolution global maps of 21st-century forest cover change. Science, 342(6160), 850–853. https://doi.org/10.1126/science.1244693

Herrmann, S. M., Tappan, G. G., & Forget, Y. (2020). Accelerating land cover change in West Africa over four decades. Communications Earth & Environment, 1, 64. https://doi.org/10.1038/s43247-020-00053-y

Herrmann, S. M., Tappan, G. G., & Forget, Y. (2020). Accelerating land-cover change in West Africa over four decades. Communications Earth & Environment, 1, 64. https://doi.org/10.1038/s43247-020-00053-y

Hijmans, R. J. (2023). terra: Spatial data analysis. R package version 1.7-78. https://CRAN.R-project.org/package=terra

Ibrahim, H., Abdulkadir, A., & Abdullahi, H. S. (2021). Land use/land cover change detection and implications for sustainable agriculture in northern Nigeria. *Environmental Challenges, 5*, 100269. https://doi.org/10.1016/j.envc.2021.100269

Jiang, Z., Lian, X., Qiu, B., Wu, J., & Chen, Y. (2020). Fire regimes and vegetation dynamics in tropical savannas under changing climate. *Science of the Total Environment, 711*, 134581. https://doi.org/10.1016/j.scitotenv.2019.134581

Koko, A. F., Raimi, M. O., Ayeni, A. O., & Ayanlade, A. (2021). Analyzing urban growth and land cover change scenario in Lagos, Nigeria. Geomatics, Natural Hazards and Risk, 12(1), 1310–1335. https://doi.org/10.1080/19475705.2021.1887940

Leroux, L., Bégué, A., Lo Seen, D., Jolivot, A., & Kayitakire, F. (2021). Using MODIS time series to monitor land-cover dynamics in Sub-Saharan Africa. *International Journal of Applied Earth Observation and Geoinformation, 95*, 102254. https://doi.org/10.1016/j.jag.2020.102254

Li, G., Li, X., Ciais, P., Yue, C., & Chen, J. (2022). Global impacts of future urban expansion on terrestrial biodiversity. Nature Communications, 13, 1642. https://doi.org/10.1038/s41467-022-29324-2

Li, G., Li, X., Ciais, P., Yue, C., & Chen, J. (2022). Global impacts of future urban expansion on terrestrial biodiversity. Nature Communications, 13, 1642. https://doi.org/10.1038/s41467-022-29324-2

Li, W., MacBean, N., Ciais, P., Defourny, P., Lamarche, C., Bontemps, S., ... & Hartley, A. (2018). Gross and net land cover changes in the main plant functional types derived from the annual ESA CCI land cover maps (1992–2015). Earth System Science Data, 10, 219–234. https://doi.org/10.5194/essd-10-219-2018

Li, W., MacBean, N., Ciais, P., Defourny, P., Lamarche, C., Bontemps, S., ... & Hartley, A. (2018). Gross and net land cover changes in the main plant functional types derived from the annual ESA CCI Land Cover maps (1992–2015). Earth System Science Data, 10(1), 219–234. https://doi.org/10.5194/essd-10-219-2018

Midekisa, A., Holl, F., Savory, D. J., & Senay, G. B. (2020). Integrating multi-sensor data for land-cover classification in sub-Saharan Africa. *Remote Sensing Applications: Society and Environment, 18*, 100314. https://doi.org/10.1016/j.rsase.2020.100314

Nwosu, C. O., Udo, S. O., & Akinyemi, F. O. (2023). Land use dynamics and vegetation productivity trends in northern Nigeria savannas from 2001–2021. *Environmental Monitoring and Assessment, 195*, 845. https://doi.org/10.1007/s10661-023-11450-8

Oluseyi, F., Olayinka, D., & Eguavoen, I. (2020). Urban growth and climate vulnerability in West African coastal cities. *Urban Climate, 33*, 100667. https://doi.org/10.1016/j.uclim.2020.100667

Padarian, J., Minasny, B., & McBratney, A. B. (2022). Data fusion for global soil and land-cover mapping using deep learning. *Geoderma, 422*, 115953. https://doi.org/10.1016/j.geoderma.2022.115953

Papa, F., Prigent, C., Aires, F., Jimenez, C., Rossow, W. B., & Matthews, E. (2010). Interannual variability of surface water extent at the global scale, 1993–2004. *Journal of Geophysical Research, 115*(D12), D12111. https://doi.org/10.1029/2009JD012674

Samaké, M., Tappan, G., Herrmann, S., & Diouf, A. (2023). Agricultural expansion and savanna transformation in West Africa: Insights from 40 years of Landsat observations. *Land, 12*(2), 289. https://doi.org/10.3390/land12020289

Simwanda, M., & Ranagalage, M. (2021). Monitoring urban sprawl and its impacts on land surface temperature in Africa's rapidly growing cities. *Urban Science, 5*(2), 41. https://doi.org/10.3390/urbansci5020041

Sulla-Menashe, D., & Friedl, M. A. (2018). User guide to collection 6 MODIS land cover (MCD12Q1 and MCD12C1) product. *NASA MODIS Land Science Team.* https://lpdaac.usgs.gov/products/mcd12q1v006

United Nations Convention to Combat Desertification (UNCCD). (2023). Report from Nigeria—UNCCD National Report 2022 (NGA). https://www.unccd.int/sites/default/files/national-reports/2022/NGA/UNCCD%20National%20Report%202022%20NGA.pdf

United Nations Department of Economic and Social Affairs (UN DESA). (2021). Sustainable Development Goal 15: Life on land. https://sdgs.un.org/goals/goal15